

See discussions, stats, and author profiles for this publication at: <https://www.researchgate.net/publication/236214265>

# Ultra-Low-Temperature Epitaxy of Ge-based Semiconductors and Optoelectronic Structures on Si(100): Introducing Higher Order Germanes (Ge<sub>3</sub>H<sub>8</sub>, Ge<sub>4</sub>H<sub>10</sub>)

**DATASET** *in* CHEMISTRY OF MATERIALS · MARCH 2012

Impact Factor: 8.35 · DOI: 10.1021/cm3002404

---

CITATIONS

17

---

READS

48

## 7 AUTHORS, INCLUDING:



**Liying Jiang**

IBM

27 PUBLICATIONS 232 CITATIONS

SEE PROFILE



**Richard T Beeler**

Arizona State University

41 PUBLICATIONS 509 CITATIONS

SEE PROFILE



**Tylan Strike Watkins**

Arizona State University

13 PUBLICATIONS 83 CITATIONS

SEE PROFILE



**A. Chizmeshya**

Arizona State University

160 PUBLICATIONS 2,364 CITATIONS

SEE PROFILE

# Ultra-Low-Temperature Epitaxy of Ge-based Semiconductors and Optoelectronic Structures on Si(100): Introducing Higher Order Germanes ( $\text{Ge}_3\text{H}_8$ , $\text{Ge}_4\text{H}_{10}$ )

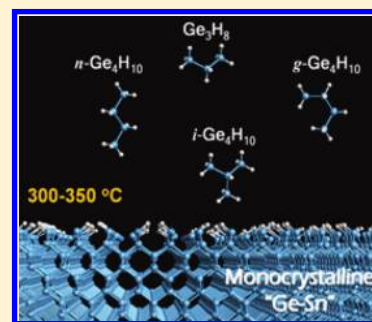
Gordon Grzybowski, Liying Jiang, Richard T. Beeler, Tylan Watkins, Andrew V. G. Chizmeshya, Chi Xu, José Menéndez, and John Kouvetakakis\*

Department of Chemistry and Biochemistry and Department of Physics, Arizona State University, Tempe, Arizona 85287-1604, United States

## S Supporting Information

**ABSTRACT:** This paper reports the development and optimization of an enhanced process to produce viable quantities of trigermene, and controlled smaller quantities tetragermene, which are isolated as a mixture of perfectly stable isomers. The identity and fundamental structural properties of these higher order germanes ( $\text{Ge}_3\text{H}_8$ , and  $\text{Ge}_4\text{H}_{10}$  isomers) are thoroughly characterized using spectroscopic methods and quantum chemical simulations. These hydride products are found to exhibit a remarkably good stability and “ease of use”, making them compatible with current industry standards. As a proof-of-concept, we demonstrate that  $\text{Ge}_3\text{H}_8$  and  $\text{Ge}_4\text{H}_{10}$  both represent efficient and cost-effective precursors for ultra-low-temperature chemical vapor deposition of pure Ge and GeSn alloy films directly on Si(100) wafers, at conditions compatible with processes currently employed in next-generation group IV device designs. In the case of Ge the crystallinity of the resultant films is found of optical quality, in spite of the extremely low temperature processing, suggesting the potential for rapid adoption of the new processes into the device application arena. In the case of GeSn alloys, the high growth rates achieved at low temperatures ( $\sim 300^\circ\text{C}$ ) allow the formation of highly concentrated bulk-like layers with unprecedented thicknesses compatible with Si-based photonic applications such as infrared (IR) emitters and detectors directly on Si wafers.

**KEYWORDS:** trigermene, tetragermene, IR optoelectronics, Ge on Si, GeSn alloys,



## 1. INTRODUCTION

Germane is the most commonly used hydride for the chemical vapor deposition of Ge-based materials and devices for applications in group IV microelectronic and optoelectronic technologies. The compound is widely available at the industrial scale in high purity form, and it is routinely used to create—effectively and efficiently at appropriate temperatures—polycrystalline and epitaxial Ge films on substrates via complete thermal dehydrogenation. The digermene derivative is obtained as a byproduct in the commercial synthesis of bulk germane, and it is typically utilized in niche low-temperature processing, including selective area deposition of crystalline films at high growth rates and fabrication of SiGeSn alloys under metastable conditions on silicon. The higher order trigermene has not been utilized for Ge deposition despite the expected facile reactivity, which is likely to enable ultra-low-temperature processing in high performance devices and flexible photovoltaic formats.<sup>1,2</sup>

Together, digermene and trigermene should significantly expand the process condition space available for the deposition of Ge-based materials under complementary metal oxide semiconductor (CMOS) compatible protocols. The broader temperature profile of these molecules overlaps with that of high-reactivity co-reactants, enabling the formation of kineti-

cally stabilized compounds that are only accessible at lower temperatures ( $<400^\circ\text{C}$ ).<sup>3–6</sup> In the case of digermene, the synthesis of novel direct gap Si–Ge–Sn semiconductor alloys and the introduction of low defectivity, atomically flat layers of pure Ge on Si wafers<sup>7,8</sup> represent dramatic examples of this compounds’ enhanced deposition versatility. The promising new approach to Ge-on-Si suggests that Ge can be reintroduced directly on silicon as a practical active semiconductor for the design and realization of the next generation of high speed devices.<sup>9,10</sup>

In the area of Si-photonics, the near direct-gap character of Ge has fueled a dramatic rise in global research and development of more sensitive photodetectors, high speed modulators, and laser diodes based entirely on conventional designs using Ge as the active material.<sup>11–13</sup> In the latter case, the quasi-direct condition required for lasing is achieved by the simultaneous application of tensile strain and heavy *n*-type doping of the Ge layers using chemical vapor deposition (CVD) of germanes.<sup>13</sup> From a crystal growth perspective, there is a strong demand to develop new lower temperature CVD

**Received:** January 21, 2012

**Revised:** March 15, 2012



routes to replace state-of-the-art methods traditionally used to control defect microstructure and layer morphology.<sup>1,7,14</sup> For example, post-growth annealing cycles in these technologies invariably produce extended defects due to the thermal mismatch with silicon, while the high-temperature step used to accelerate growth following the initial low temperature layer deposition also induces strains, defects, and cracks, which ultimately degrade the material performance.<sup>8,15</sup>

An alternative route to direct gap group IV materials for applications in Si photonics is alloying Ge with modest concentrations of Sn in the 6–12% range.  $\text{Ge}_{1-x}\text{Sn}_x$  alloys have been grown directly on Si(100) using CVD reactions of  $\text{Ge}_2\text{H}_6$  and  $\text{SnD}_4$ , and films with low Sn contents (<3%) have been used to fabricate prototype photodetectors exhibiting enhanced performance relative to Ge analogs. The results of these studies indicate that the next generation of device structures for applications in lasers and solar cells would require the development of new deposition processes that may contribute to a dramatic increase of the growth rates, as well as the expansion of the range of Sn concentrations at low temperatures.

In both the Ge and GeSn cases, the ideal growth processes should efficiently convert gas-phase Ge into thick, optical quality Ge-based films on silicon at the highest possible, most cost-effective growth rates (commercial scale) but lowest possible temperatures to avoid the materials issues noted for Ge and in addition, Sn segregation in the case of GeSn. The foregoing indicates that higher order germanes with enhanced reactivity such as trigermane, which is predicted to exhibit a reasonable vapor pressure of ~25 Torr at room temperature, may represent suitable candidates for the development for such processes.

Higher order hydrides have already made a significant contribution in the silicon technology space, where the trisilane analog (available under the trade name Silcore)<sup>16,17</sup> or even the heavier neopentasilane<sup>14</sup> have been successfully used to enhance deposition processes in the industrial sector. In this connection, trigermane is not yet commercially available as a chemical source for applications in group IV materials science, presumably due to the lack of practical synthesis methods to produce sufficient amounts of the pure product. The best known (widely reported) synthesis of trigermane was conducted almost 40 years ago via an electric discharge decomposition of germane gas, resulting in low yields of the main product intermixed with higher mass analogs that were tentatively identified as tetragermane and pentagermane.<sup>18,19</sup> The poor production rate and the complicated experimental setup makes this method difficult to implement for large-scale production of semiconductor grade material, as required for crystal growth applications. Nevertheless, sufficient quantities of the compound were obtained to allow some basic characterizations and preliminary demonstration of the molecular synthesis of its halide derivatives.<sup>20,21</sup>

Prior mechanistic studies involving insertion reactions of silylenes and germylenes into Si–Si and Ge–Ge bonds have identified the formation of trace amounts of trisilane and trigermane byproducts by thermal decomposition of their lower order counterparts. However, the isolation of the compounds for bulk analysis or subsequent use was apparently not pursued.<sup>22</sup> Another reason for limited use of higher-order germanes may be related to the purported instability of  $\text{Ge}_2\text{H}_6$ , which have prevented its availability in pure liquid state and have cast uncertainty for the potential development and

possible deployment of the even more reactive  $\text{Ge}_3\text{H}_8$  as a potential laboratory reagent and, perhaps more importantly, as a commercial semiconductor source. In fact, the open literature offers very limited information regarding the fundamental thermodynamic and structural properties of  $\text{Ge}_3\text{H}_8$ , as well as the determination of its physical behavior.

The focal point of our study was to develop a practical synthesis route that allows the isolation of significant amounts of the  $\text{Ge}_3\text{H}_8$ , enabling a thorough characterization and its application as a viable ultra-low-temperature deposition source for the fabrication of Ge-based semiconductors on Si. Our first synthetic attempts employed a thermolysis reaction of digermane, as described by the following equation, to obtain a high yield of the pure product in gram quantities, allowing a determination of its physical behavior and stability range.



Several years ago, an analogous reaction to produce bulk trisilane from disilane was described in the patent literature for use in semiconductor fabrication.<sup>23</sup> In the presented idealized reaction, two moles of digermane dissociate to yield equimolar amounts of germane and trigermane, implying a maximum theoretical yield of 50% product and  $\text{GeH}_4$  byproduct, which contains the remaining balance of Ge. In principle, the  $\text{GeH}_4$  can be completely recycled with no net loss, thereby also making the process cost-effective for bulk production, as needed in large scale crystal growth applications. In this paper, we show that the reaction generates trigermane as the primary decomposition product. The trigermane is isolated from the main  $\text{GeH}_4$  byproduct and then purified as a colorless, volatile liquid. This process also yields a small amount of tetragermane (butane analog with enhanced reactivity), which was isolated as a mixture of perfectly stable isomers, as shown in Figure 1.

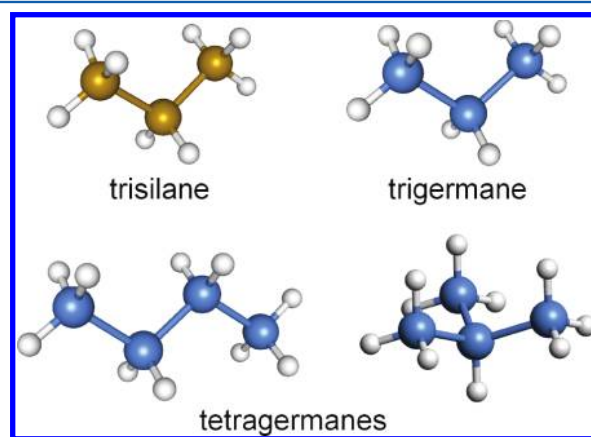


**Figure 1.** Molecular structures of trisilane ( $\text{Si}_3\text{H}_8$ ), trigermane ( $\text{Ge}_3\text{H}_8$ ), and the two tetragermane ( $\text{Ge}_4\text{H}_{10}$ ) isomers produced in this study. Legend: Si (gold), Ge (blue), H (white).

Significant quantities of the compounds were obtained and were found to be perfectly stable, allowing a full characterization using modern experimental and theoretical methods, in order to elucidate their fundamental structural, vibrational, and thermodynamic properties. In this study, samples of pure trigermane and tetragermane were subsequently employed to conduct proof-of-concept depositions of Ge and GeSn films on Si wafers. The initial results are highly encouraging and indicate that the growth rate of pure Ge on Si using  $\text{Ge}_4\text{H}_{10}/\text{Ge}_3\text{H}_8$  is significantly enhanced—up to 20 times for  $\text{Ge}_4\text{H}_{10}$ , depending

on the conditions—over the current state-of-the-art process using digermene under the same conditions.<sup>29</sup> In addition, the rapid formation of high-Sn content GeSn films on Si(100) has been observed using significantly reduced amounts of the precursor relative to Ge<sub>2</sub>H<sub>6</sub>, indicating that the conversion of gaseous Ge hydride into solid material proceeds with higher efficiency. Furthermore, in both cases, the crystal quality of the resultant films is comparable to the best results obtained using Ge<sub>2</sub>H<sub>6</sub>, suggesting that the learning curve for the translation of the new trigermene-based process into the device arena will be extremely rapid. Finally, we show that tetragermene provides the ultimate pathway for the formation of Ge-on-Si structures with the desired optical and materials properties. We speculate that further gains will be difficult to realize using chemical means. The results suggest that compound is likely to be a suitable source for a wide range of applications requiring a high reactivity Ge source including direct write of nanoscale structures using scanning probe methods.

## 2. EXPERIMENTAL, RESULTS, AND DISCUSSION

The pyrolysis reactor comprises of a 1 in. Pyrex tube packed with glass wool and heated by a “clam shell” resistance furnace with a nominal hot zone of ~12 in. long (see the Supporting Information). The exhaust of the tube is connected in series to two sequential glass traps cooled to −196 °C, which can be individually isolated using high vacuum valves. The inlet of the tube is connected to a bubbler typically charged with several grams of liquid digermene, typically held at a target temperature of −30 °C. Under these conditions, the vapor pressure of Ge<sub>2</sub>H<sub>6</sub> is ~25 Torr, which is sufficient to permit controlled transport of the vapor into the reactor assuming that high purity H<sub>2</sub> as a carrier gas is fully saturated. The flow of H<sub>2</sub> is regulated using a calibrated flow meter so that both the amount of reactant and its retention time in the reactor can be adjusted as needed to optimize the reaction conditions and maximize yields of the products.

Both the bubbler and the terminal trap are connected to a high vacuum line to allow differential pumping of the entire system before and after the pyrolysis experiment and also transfer and collection of the final products and unused reactant. The vacuum line is equipped with several capacitance manometers to accurately measure pressures in the range 0.1–1000 Torr and a mercury bubbler that serves as a “release valve” to vent the H<sub>2</sub> carrier gas overpressure from the closed loop system. The mercury in the bubbler prevents atmospheric back flow ensuring that the entire process is carried out under inert conditions and a total pressure of 760 Torr. A reaction temperature of 225 °C yielded no measurable decomposition of digermene under our reaction conditions (H<sub>2</sub> flow rate, etc.) as evidenced by almost full recovery of the starting material, no visual change in the appearance of the tube and packing material. Increasing the temperature to 250 °C resulted in significant condensation of products in both traps and the formation of a very thin metallic coating inside the tube, presumably due to the formation of Ge-like residue.

Upon completion, the cold traps containing the products and any unreacted source material are isolated from the pyrolysis chamber, pumped to remove the H<sub>2</sub> ambient (note that H<sub>2</sub> does not condense at −196 °C) and then warmed to room temperature while monitoring their pressure using the in-line manometers. The combined volatile content from both traps is then separated through fractionation to isolate the individual components of the pyrolysis mixture. Germane, trigermene, and

digermene are collected by distillation via trap-to-trap fractionation at −196, −110, and −78 °C respectively. In addition, a small amount of colorless mobile liquid with a nominal vapor pressure of 1.5 Torr is typically recovered at a −35 °C trap and has been identified as tetragermene. Pure trigermene is also obtained as a colorless liquid with a room temperature vapor pressure of 21 Torr, close to the predicted 25 Torr value. Under these conditions, the dissociation of ~2.5 g of digermene yielded ~1.0 g of trigermene, which represents a 55% yield on the basis of the idealized reaction. In addition, we produced ~0.30 g of tetragermene as well as 0.90 g of germane, indicating the presence of more complex reactions channels under the current protocols. Nevertheless, our experiments thus far represent a very small excursion in a very wide parameter space that includes temperature, pressure, retention time, mass flow, tube diameter and type (glass vs metal), length of hot zone, packing medium, etc. All of these parameters can, in principle, be adjusted to maximize yield using our present results as a starting point. The relatively high yield obtained thus far is encouraging and indicates that further improvements of the process output may be within reach.

The collective output from several reaction runs provided sufficient amounts of material (~7 g) to enable a series of deposition studies using trigermene as chemical source for the first time. In addition, 1.5 g of tetragermene was also collected. Both of these products were stored in glass vessels at room temperature and exhibited no visible color change or other signs of decomposition. However, in the case of tetragermene, infrared (IR) spectroscopy revealed trace amounts of germane over the span of approximately 1–2 months.

The structural properties of the molecules and the purity of all samples were investigated by NMR spectroscopy using a 500 MHz Varian spectrometer, and the results obtained appeared consistent with those reported in early synthetic studies.<sup>20</sup> However, the superior quality of our samples and the availability of higher resolution NMR techniques clearly illustrates the perfect analogy with propane and butane structures and conformations for the first time. In the case of trigermene, the <sup>1</sup>H spectrum showed two sets of peaks corresponding to a triplet at 3.273 ppm, integrated for six protons, as well as a septet at 3.18 ppm, integrated for two protons, as expected due to the terminal GeH<sub>3</sub> and the bridged GeH<sub>2</sub> moieties, respectively. The <sup>1</sup>H spectrum of the tetragermene sample indicated a mixture of the two configurational isomers with resonances exhibiting the appropriate multiplicities (see Figure 2). The peaks of the *n*-Ge<sub>4</sub>H<sub>8</sub> (straight chain) appeared as a triplet at 3.273 pp and a quartet at 3.18 ppm corresponding to the central GeH<sub>2</sub>–GeH<sub>2</sub> and terminal GeH<sub>3</sub> fragments of the molecule. Both peaks are significantly broadened due to the presence of the *gauche* and *trans* conformers, reminiscent of those observed in the classic *n*-butane proton spectrum. In contrast, the resonances of the *i*-Ge<sub>4</sub>H<sub>8</sub> are sharp and distinct, and they appeared as a doublet at 3.384 ppm and a decet at 2.868 ppm, integrating for 9 and 1 protons, respectively, as expected. These assignments were confirmed by 2-D COSY (two-dimensional correlation spectroscopy) NMR. The combined integrated intensities of the peaks in the spectra indicated that the normal- and iso-species are typically present in a ~5:1 ratio in our samples.

The preceding isomeric ratio is, in fact, very similar to that obtained for liquid mixtures of commercially available tetrasilanes (Voltaix Corp), in which all of the same structural/composition conformers are present. However, the



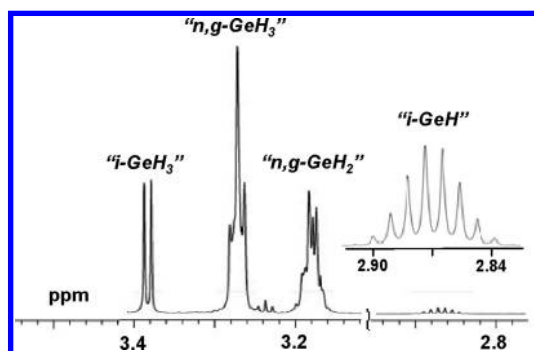


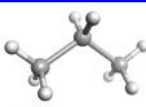
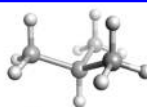
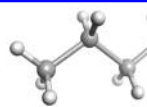
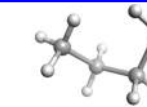
**Figure 2.** 500 MHz  $^1\text{H}$  spectrum of the isomeric tetragermane mixture showing resonances corresponding to the various  $\text{GeH}_x$  moieties of the  $i\text{-GeH}(\text{GeH}_3)_3$  as well as the  $n$ - and  $g$ - conformers of  $\text{GeH}_3\text{GeH}_2\text{GeH}_2\text{GeH}_3$ . The inset is a magnified view of the Ge–H resonance of the iso-compound at 2.7 ppm. The  $^1J$  coupling constants from left to right are 4.28, 4.52, 4.64, and 4.41 Hz. The weak triplet in the vicinity 3.28 ppm is due to residual traces of trigermane.

proportions of isomers in the gas phase are expected to differ from those of the liquid, and therefore, the isomeric composition of the gas phase flux used as a CVD source will have a significant effect on the design and interpretation of film deposition, including layer morphology, kinetics of film assembly, and other key crystal growth properties. In fact, it is remarkable that detailed studies comparing the properties of high-order group IV hydrides of Si and Ge with their classic butane analog are scarce, even though the similarities are quite apparent. For this reason, we have carried out in-depth characterizations of the vibrational and configurational behavior of gas phase trigermane and tetragermane using IR spectroscopy and quantum chemical simulations. The latter support the identification of the molecules and provide a rigorous vibrational and thermodynamic basis for establishing the more elusive isomeric proportions in the case of tetragermane.

**Quantum Chemical Simulations of Structural, Vibrational, and Thermochemical Properties.** In prior studies, we demonstrated that B3LYP hybrid density functional theory (DFT) simulations provide an excellent account of the ground state structural, thermochemical, and vibrational properties of the  $(\text{H}_3\text{Ge})_n\text{SiH}_{4-n}$  and butane-like Si–Ge hydride family of molecules.<sup>24,25</sup> In the present work, the ground state properties of trigermane and tetragermane isomers were calculated using density functional theory (DFT), as implemented in the Gaussian03 code.<sup>26</sup> We follow our prior work in adopting the B3LYP hybrid exchange–correlation functional in conjunction with a standard 6-311G++(3df,3pd) basis set. Using so-called “very tight” structural convergence criteria and “ultrafine” integration grids and without imposing any symmetry constraints, our simulations yielded the static ground state molecular structures listed in Table 1. In all cases, all harmonic normal-mode frequencies were calculated to be positive definite, indicating that the ground state structures are dynamically stable. A symmetry analysis of the final structures yielded  $C_{2v}$ ,  $C_{3v}$ ,  $C_{2h}$ , and  $C_2$  point groups for the  $\text{Ge}_3\text{H}_8$ ,  $i\text{-Ge}_4\text{H}_{10}$ ,  $n\text{-Ge}_4\text{H}_{10}$ , and  $g\text{-Ge}_4\text{H}_{10}$  molecules, respectively.

The bond lengths obtained from our simulations follow the expected trends and are in excellent agreement with those obtained by other authors, and those reported in our prior work on trigermane and tetragermane<sup>27</sup> using slightly smaller basis sets and coarser grids. For example, the shortest Ge–Ge bond lengths (2.444 Å) typically occur between  $-\text{GeH}_3$  and  $-\text{GeH}_2-$  moieties, while slightly longer values (2.450 Å) prevail between  $-\text{GeH}_3$  and  $-\text{GeH}-$ , or adjoining  $-\text{GeH}_2-$  groups. The Ge–H bond lengths follow the expected increasing trend 1.537 Å, 1.542 Å, and 1.545 Å for the  $-\text{GeH}_3$ ,  $-\text{GeH}_2-$ , and  $-\text{GeH}-$  moieties, respectively. The bond angle trends in these molecules also exhibit systematic patterns with typical  $\angle\text{Ge}-\text{Ge}-\text{Ge}$  angles of  $113.1^\circ$  among the molecules/isomers containing a  $C_2$  symmetry character but a more tetrahedral value of  $110.5^\circ$  in the case of the  $i\text{-Ge}_4\text{H}_{10}$  species possessing

**Table 1.** Summary of Structural and Energetic Results for Trigermane and Three Isomers of Tetragermane<sup>a</sup>

		 <b>Trigermane</b> $(\text{Ge}_3\text{H}_8)$	 <b>iso-Tetragermane</b> $(i\text{-Ge}_4\text{H}_{10})$	 <b>n-Tetragermane</b> $(n\text{-Ge}_4\text{H}_{10})$	 <b>g-Tetragermane</b> $(g\text{-Ge}_4\text{H}_{10})$
<b>Point Group</b>		$C_{2v}$	$C_{3v}$	$C_{2h}$	$C_2$
<b>Bond Lengths</b> (Å)	Ge–Ge	2.444	2.450	2.445(×2), 2.449	2.444(×2), 2.451
	(Ge–H) <sub>T</sub>	1.537 (×3)	1.538(×3)	1.537(×2), 1.538	1.537(×2), 1.538
	(Ge–H) <sub>S</sub>	1.541	1.545*	1.542	1.542
<b>Bond angles</b> (degrees)	$\angle\text{Ge}-\text{Ge}-\text{Ge}$	112.9	110.5	113.1	113.1
	(H–Ge–H) <sub>T</sub>	108.4, 108.5(×2)	108.4(×2), 108.5	108.4, 108.5(×2)	108.4, 108.5(×2)
	(H–Ge–H) <sub>S</sub>	107.2	--	107.1	107.3
<b>Dipole Moment (D)</b>		0.0389	0.0708	0.0000	0.0361
<b>Thermochemistry</b> ( $T=298\text{K}$ , $P=1\text{atm}$ )	$E_0$ (a.u.)	-6235.86419	-8314.09421	-8314.09378	-8314.09316
	$E_0+E_{\text{th}}$ (a.u.)	-6235.79414	-8314.00513	-8314.00435	-8314.00407
	$E_0+H_{\text{th}}$ (a.u.)	-6235.79319	-8314.00419	-8314.00341	-8314.00312
	$E_0+G_{\text{th}}$ (a.u.)	-6235.83725	-8314.05737	-8314.05526	-8314.05483
	S (cal/mol K)	92.73	111.93	109.12	108.83

<sup>a</sup>The subscripts T and S refer to terminal and sagittal H–Ge–H bond angle species. The asterisk on the (Ge–H)<sub>S</sub> bond length in  $i\text{-Ge}_4\text{H}_{10}$  indicates that the  $-\text{Ge}-\text{H}$  moiety is distinct from the other sagittal  $-\text{GeH}_2-$  moieties.

$C_{3v}$  symmetry. While the torsion angle among the Ge atoms adopts trivial values for the high symmetry species, we obtain  $58^\circ$  for the gauche tetragermane isomer, which is quite close to the typical  $63^\circ$  value found in the gauche isomer of butane.<sup>28</sup> The dipole moments of the molecules corresponding to the equilibrium ground structures described (listed in Table 1) indicate a maximum value of 0.071 D for the *i*-Ge<sub>4</sub>H<sub>10</sub> molecule, similar values in the range of  $\sim 0.32$ – $0.36$  for Ge<sub>3</sub>H<sub>8</sub> and *g*-Ge<sub>4</sub>H<sub>10</sub>, and a vanishing dipole moment for the *n*-Ge<sub>4</sub>H<sub>10</sub>, as expected on the basis of its symmetry.

The standard thermochemistry output from Gaussian03 at  $T = 298$  K and  $P = 1$  atm is also summarized in our table and includes the static electronic energy of the molecules,  $E_0$ , as well as its thermally corrected counterparts for internal energy ( $E_{th}$ ), enthalpy ( $H_{th}$ ), and free-energy ( $G_{th}$ ). A key outcome of these calculations for the tetragermanal species is that the *i*-Ge<sub>4</sub>H<sub>10</sub> has the lowest free-energy (by  $\sim 4.4$  kJ/mol), followed by *n*-Ge<sub>4</sub>H<sub>10</sub> and *g*-Ge<sub>4</sub>H<sub>10</sub>, whose free-energies differ by a mere  $\sim 1$  kJ/mol. These free-energies are used to develop a simple isomerization model. Finally, our table lists the molecular entropies of the molecules obtained at  $T = 298$  K for trigermane and the tetragermane isomers. In view of its relatively weak mass dependence, the translational component of the entropy ( $\sim 43$  cal/(mol K)) is approximately the same for all molecules and the overall magnitude of the total entropy is essentially controlled by the vibrational term, which is  $\sim 14.6$  cal/(mol K) for trigermane and typically 35–39 cal/(mol K) for the tetragermane isomers, with *i*-Ge<sub>4</sub>H<sub>10</sub> being dominant. By contrast, the largest rotational term occurs in the *n*-Ge<sub>4</sub>H<sub>10</sub>, due to its larger moment of inertia.

As shown in Figure 3, the calculated vibrational spectrum of trigermane is separated into two categories corresponding to high-frequency Ge–H stretching vibrations ( $2000$ – $2150$  cm<sup>−1</sup>)

and lower frequency Ge–H wagging and bending motions, as well as Ge–Ge–Ge backbone vibrations ( $<1200$  cm<sup>−1</sup>). Based on our prior work on closely related Si–Ge hydrides calculated using the same methodology, we reconcile the differences between the observed frequencies and those calculated using well-established scale factors 0.995 and 0.975 for the low and high frequency ranges, respectively. The corresponding plots of our calculated spectra are compared directly with those measured experimentally in Figure 3, and indicate generally good agreement. The lowest frequency normal modes, labeled  $\nu_1$ – $\nu_3$  in the figure are assigned as follows:  $\nu_1$ , in-phase GeH<sub>3</sub>/GeH<sub>2</sub> wagging  $\parallel$  (e.g., parallel) to backbone;  $\nu_2$ , antiphase wagging of the GeH<sub>3</sub>/GeH<sub>2</sub>  $\parallel$  to backbone. The most intense IR modes are labeled as  $\nu_3$ – $\nu_7$  and are assigned as follows:  $\nu_3$ , intense GeH<sub>2</sub> wagging  $\parallel$  to backbone;  $\nu_4$ , intense in-phase GeH<sub>2</sub> wagging  $\parallel$  to backbone;  $\nu_5$ , intense antiphase GeH<sub>2</sub> wagging  $\parallel$  to backbone;  $\nu_6$ , this band contains three very closely spaced frequencies corresponding to in-phase wagging of the terminal –GeH<sub>3</sub> protons  $\perp$  (e.g., perpendicular) to backbone ( $\nu_6$ ), as well as an in-phase and antiphase pair of vibrations involving scissor-like GeH<sub>3</sub> motion  $\perp$  to the backbone. We note that the calculated trigermane spectrum does not produce any vibrational modes in the vicinity of the  $700$  cm<sup>−1</sup> feature observed experimentally. However, this peak has, in fact, been observed in some of the first spectra recorded for this molecule, suggesting that the absorption is inherent to the pure compound. Furthermore, the NMR spectra of trigermane indicate that the bulk sample is highly pure thereby precluding the assignment of this peak to a contaminant/impurity. A possible origin for the  $700$  cm<sup>−1</sup> feature is a combination band, but a complete analysis of this mechanism is beyond the scope of the present study.

The higher frequency portion of our calculated spectrum is shown in the lower panel of Figure 3 and indicates a complex band of frequencies corresponding to symmetric and antisymmetric Ge–H stretches in various in-phase and antiphase combinations. For example, the most intense features labeled as  $\nu_{10}$  correspond to in-phase but antisymmetric H–Ge–H modes within the –GeH<sub>3</sub> groups, while  $\nu_8$  contains closely spaced frequencies corresponding to symmetric and asymmetric stretches of the bridging –GeH<sub>2</sub>– moiety. Finally, the mode designated as  $\nu_9$  is associated with in-phase asymmetric stretching of Ge–H bonds in the terminal –GeH<sub>3</sub> groups. The comparisons with experiment corroborate the high degree of purity of the gas phase product, which is consistent with the “text-book” NMR spectrum of the corresponding propane-like liquid phase, completely devoid of any impurity signatures.

**Thermochemistry of Tetragermanes.** In the case of tetragermane, we consider the existence of classic butane-like isomerization comprised of two conformational isomers (“trans” and “gauche”, referred to from here simply as *n*-Ge<sub>4</sub>H<sub>10</sub> and *g*-Ge<sub>4</sub>H<sub>10</sub>) and one positional isomer analogous to iso-butane (referred to as *i*-Ge<sub>4</sub>H<sub>10</sub>). The predominance of any one isomer in the gas phase has important implications for the use of tetragermane as a deposition source in CVD growth of Ge-based materials. It is expected that the most thermodynamically stable configuration will lead to the most facile assembly of crystalline Ge at ultra low-temperatures. This is manifested in the analogous growth of silicon on Si(100) using the neopentasilane sources,<sup>14</sup> which purportedly decompose on the surface via the formation of iso-tetrasilane intermediates. According to the thermochemical data in Table 1 the most

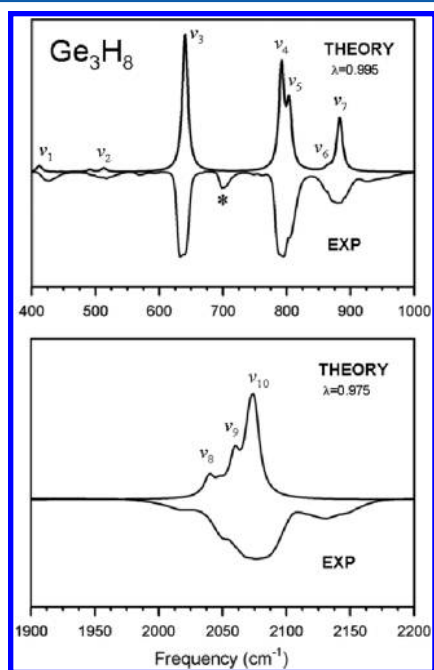


**Figure 3.** Comparison of the calculated and experimental IR spectrum for trigermane. Primary spectral features are designated  $\nu_1$ – $\nu_{10}$  and discussed in the text. The frequencies of simulated spectra were scaled by factors of 0.995 and 0.975 in low- and high-frequency ranges, respectively.

stable species is  $i\text{-Ge}_4\text{H}_{10}$ , which is consistent with the trends observed in classic butane, where simple gas phase models predict a room temperature equilibrium ratio of  $\sim 9:1$  for  $i\text{-C}_4\text{H}_{10}/n\text{-C}_4\text{H}_{10}$ .<sup>27</sup> The calculated vibrational spectra of the tetragermane isomers are shown in Figure 4 (top and bottom

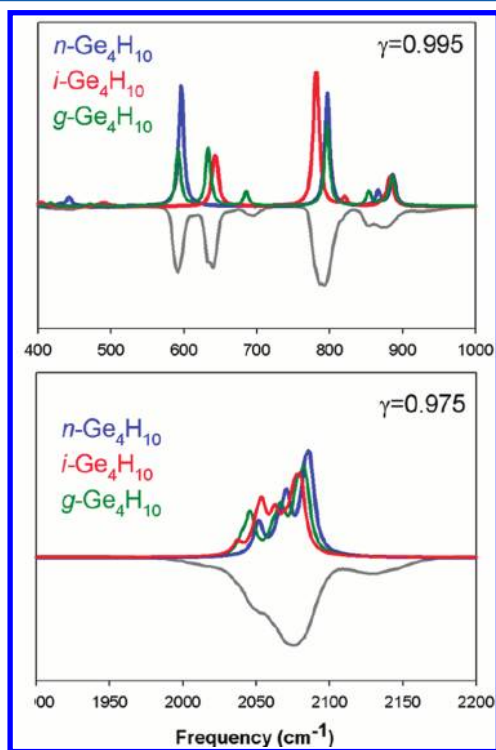
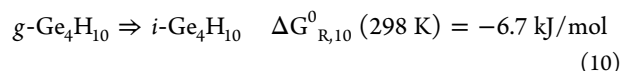
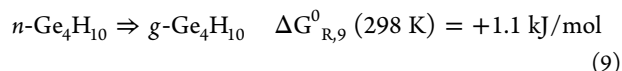
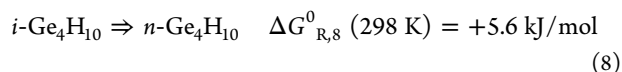


**Figure 4.** Low- and high-frequency IR spectra of the individual isomers used to construct the composite spectrum. The individual frequency scale factors ( $\gamma$ ) are the same as those employed in the trigermane calculations (Figure 2).

corresponding to low- and high-frequency regimes), where they are compared with an experimental spectrum of a gas sample. The latter was obtained from a freshly distilled bulk liquid aliquot which was previously characterized by NMR spectroscopy, showing a mixture of 85%  $n\text{-Ge}_4\text{H}_{10}$  and 15% of  $i\text{-Ge}_4\text{H}_{10}$ , where the 85% can, in principle, be further subdivided into “trans” and “gauche”, which can not be clearly resolved by NMR spectroscopy. We note, however, that the presence of two isomers in the dominant fraction is consistent with the broadening of the NMR signals for the  $n\text{-Ge}_4\text{H}_{10}$  species. The simulated gas phase IR spectra shown in Figure 4 (top) clearly indicate that the spectral signatures of the individual isomers are unique and fairly well resolvable. For example, the intense band in the vicinity of  $600\text{ cm}^{-1}$  originates mainly from an intense  $n\text{-Ge}_4\text{H}_{10}$  vibration associated with in-phase  $\text{GeH}_3/\text{GeH}_2$  wagging  $\parallel$  to  $\text{Ge}_4$  backbone, while the strongest absorption near  $780\text{ cm}^{-1}$  is due to  $\text{GeH}_3$  wagging  $\parallel$  to a  $\text{Ge-Ge}$  bond axis in  $i\text{-Ge}_4\text{H}_{10}$ , where the apparent broadening is due to the close coincidence of the latter with another normal of  $n\text{-Ge}_4\text{H}_{10}$  occurring near  $800\text{ cm}^{-1}$  due to in-phase  $\text{GeH}_3$  wagging  $\parallel$  to backbone. The spectra also show that the complex band near  $640\text{ cm}^{-1}$  is due to wagging motions of the lone  $\text{Ge-H}$  at the tertiary site, which is entirely unique to the  $i\text{-Ge}_4\text{H}_{10}$  species. Collectively, the data described thus far clearly indicates the presence of significant amounts of  $i\text{-Ge}_4\text{H}_{10}$  in gas phase tetragermane. We note that the  $\text{Ge-H}$  bands shown in Figure 4

(bottom) are rather complex with regard to the individual isomer contributions but that the overall shape of the envelope is well reproduced by theory. More detailed peak assignments will be described elsewhere, but we refer the reader our prior work on the analogous butane-like Si-Ge hydride molecules.<sup>25</sup>

In our prior work on isomeric mixtures in butane-like Si-Ge hydride molecules, we introduced the concept of fitting a linear combination of calculated isomeric vibrational spectra to the measured spectrum of a mixture, in order to ascertain the proportions. Here, we avoid a fitting procedure and instead consider a more straightforward thermodynamic approach. From the  $E_0 + G_{\text{th}}$  values listed in Table 1, we first obtain the reaction free-energies for the three isomer interconversion reactions:



where we note that  $\sum_m \Delta G_{p,m}^0 = 0$ . Defining the extents of reaction as  $x$ ,  $y$ , and  $z$  for reactions 8, 9, and 10, respectively, simple mass balance yields the mole numbers  $n_{\text{Ti}} = n_{\text{Ti}}^0 - x + z$ ,  $n_{\text{Tn}} = x - y$ , and  $n_{\text{Tg}} = y - z$ , for the iso-,  $n$ -, and  $g$ - species, respectively. Then, assuming ideal gas behavior, the equilibrium constants are explicitly given by

$$K_{p,8}^0 = \frac{(P_{\text{Tn}}/P^0)}{(P_{\text{Ti}}/P^0)} = \frac{n_{\text{Tn}}}{n_{\text{Ti}}} = \frac{x - y}{n_{\text{Ti}}^0 - x + z},$$

$$K_{p,9}^0 = \frac{(P_{\text{Tg}}/P^0)}{(P_{\text{Tn}}/P^0)} = \frac{n_{\text{Tg}}}{n_{\text{Tn}}} = \frac{y - z}{x - y},$$

$$K_{p,10}^0 = \frac{(P_{\text{Ti}}/P^0)}{(P_{\text{Tg}}/P^0)} = \frac{n_{\text{Ti}}}{n_{\text{Tg}}} = \frac{n_{\text{Ti}}^0 - x + z}{y - z}$$

where the condition  $\sum_m \ln K_{p,m}^0 = 0$  is imposed by the cyclic nature of the reaction equations, and reduced the system to two independent equations with solutions

$$n_{\text{Ti}} = \frac{n_{\text{Ti}}^0 K_{p,10}^0}{1 + K_{p,10}^0(1 + K_{p,8}^0)},$$

$$n_{\text{Tn}} = \frac{n_{\text{Ti}}^0 K_{p,8}^0 K_{p,10}^0}{1 + K_{p,10}^0(1 + K_{p,8}^0)},$$

$$n_{\text{Tg}} = \frac{n_{\text{Ti}}^0}{1 + K_{p,10}^0(1 + K_{p,8}^0)}$$

where the total mole number is  $n_{\text{TOT}} = n_{\text{Ti}} + n_{\text{Tn}} + n_{\text{Tg}} = n_{\text{Ti}}^0$ . Substitution of the 298 K free-energies from Table 1 then yields  $K_{p,8}^0 = 0.1067$ ,  $K_{p,9}^0 = 0.6381$ , and  $K_{p,10}^0 = 14.6915$ , which, in turn, predicts an isomeric mixture consisting of  $n_{\text{Ti}} \sim 80\%$ ,  $n_{\text{Tn}} = 12\%$ , and  $n_{\text{Tg}} = 8\%$ . This is clearly in contrast with the NMR data for the liquid mixture and is quantitatively consistent with the experimental IR spectrum. To obtain a more quantitative estimate, we evaluate the equilibrium constants at the lower temperature ( $<35^\circ\text{C}$ ) from which the gas analyte was drawn. The assumption here is that the isomeric interconversion is sufficiently slow to make the lower temperature equilibrium mixture more relevant. Accordingly we re-evaluated the



thermochemistry for reactions 8–10 over the expanded range (200–600 K), yielding the equilibrium mole fraction plots shown in Figure 5a. These results indicate that the lowest free-

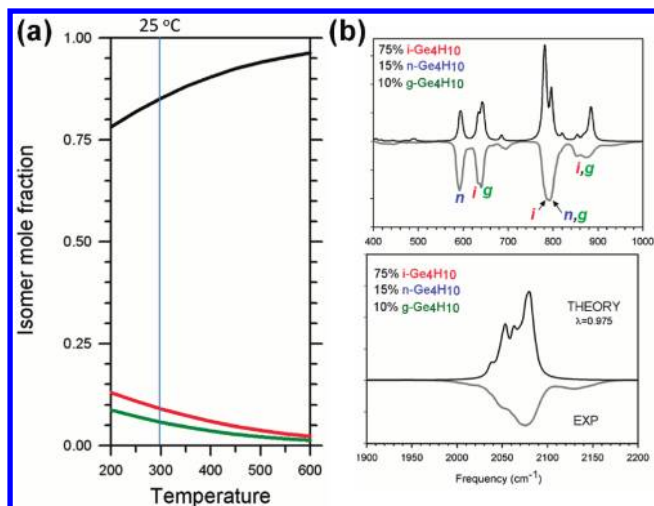


**Figure 5.** (a) Calculated temperature dependence of the tetragermane isomer mole fractions from 200 to 600 K, where the proportion of *i*-Ge<sub>4</sub>H<sub>10</sub> increases with temperature, reaching nearly ~100% at typical deposition temperatures for crystalline Ge on Si(100). (b) Composite spectrum of the tetragermane corresponding to the low-temperature combination 75%, 15%, 10% of iso-, *n*-, and *g*-species; as for the case of trigermane (Ge<sub>3</sub>H<sub>8</sub>), we applied frequency scale factors of 0.995 and 0.975 to the simulated spectra in the low- and high-frequency regimes.

energy isomer, *i*-Ge<sub>4</sub>H<sub>10</sub> (black trace), is dominant at high temperatures as expected, but that its' proportion is reduced at lower temperatures at the expense of *n*-Ge<sub>4</sub>H<sub>10</sub> (red trace) and *g*-Ge<sub>4</sub>H<sub>10</sub> (green trace) isomer species.

The infrared spectrum of tetragermane was then simulated by combining the calculated spectra of *i*-Ge<sub>4</sub>H<sub>10</sub>, *n*-Ge<sub>4</sub>H<sub>10</sub> and *g*-Ge<sub>4</sub>H<sub>10</sub>, in a 75%, 15%, 10% proportions, as shown in Figure 5b. The resulting composite spectrum compares very well with the experimental counterpart indicating that principal character (frequencies and intensities) are well accounted for. In particular, we note that a composite spectrum based on the liquid phase NMR proportions, with a dominant *n*-Ge<sub>4</sub>H<sub>10</sub> fraction, could not account for the observed gas phase spectrum.

The predominance of the *i*-Ge<sub>4</sub>H<sub>10</sub> species in the gas phase suggests that depositions could be carried out with unprecedented efficiency at low-temperatures using this source. This development may represent a key milestone toward the realization of intricate device formats via selective growth in high-speed Si–Ge based transistor structures on Si(100).

#### Growth of Ge and GeSn on Si using Trigermane.

Growth of Ge films was conducted on 3 in. Si(100) p-type wafers with resistivities of 0.01–0.02 ohms cm. The substrates were first wet-cleaned, dipped in HF to hydrogen passivate their surface, and then flashed on the sample stage to 900 °C for 1 min to obtain a clean surface as evidenced by RHEED (reflection high-energy electron diffraction). The reaction mixture was prepared by combining 15 Torr of trigermane and 300 Torr of H<sub>2</sub> in a liter container that was then attached to the reactor injection manifold and pumped to 10<sup>−8</sup> Torr. The gaseous mixture was introduced into the reactor at a constant flow using a needle valve. The substrate was heated by a ceramic element enclosed within a quartz chamber and

brought to within 0.5 cm from the wafer back side. The reaction pressure was maintained constant at 1 × 10<sup>−4</sup> Torr throughout the experiment using a corrosion resistance turbo pump. The nominal deposition temperature was estimated by subtracting ~20 °C from the reading of a thermocouple attached to the heater assembly inside the enclosure. The latter value was typically ~350 °C (no more than 10 °C lower) for all depositions. We note that the temperature of the wafer surface could not be determined using a conventional single color pyrometer operating within the IR range due to the low emissivity of Si under these conditions. The wafers stage was rotated to ensure a homogeneous distribution of the reaction flux resulting in uniform thickness profile in the films. The time frame of a typical growth was 1.5 h, producing films with thickness of 1.5 μm at growth rates of 11 nm/min, which is very high under these pressure/temperature conditions of 1 × 10<sup>−4</sup>/330 °C. As a comparison, negligible growth rates <0.5 nm/min are obtained using Ge<sub>2</sub>H<sub>6</sub> mixed with metal organic additives in our current state of the art process.<sup>29</sup> The resultant films were examined using Nomarski microscopy and found to be optically featureless, exhibiting a virtually flawless surface completely devoid of defects and imperfections. This was corroborated by atomic force microscopy (AFM) scans, which showed an rms roughness of ~2 nm over a 20 × 20 μm<sup>2</sup> area. Ellipsometry was used to determine the thickness profile, which was found to be constant 95% across the 3 in. diameter of the substrate. X-ray diffraction (XRD) on- and off-axis measurements of the as-grown material revealed a fully relaxed strain state with a bulk lattice constant of 5.658 Å and showed a 0.15° fwhm (full-width half-maximum) for the 004 rocking curve. This value indicates the formation of near state-of-the-art crystallinity in spite of the remarkably low deposition temperatures employed. Subsequent rapid thermal annealing (RTA) at 725 °C resulted in a significant narrowing of the rocking curve fwhm to a value of 0.06° for 1.5 μm thick samples. Cross-sectional transmission electron microscopy (XTEM) examinations revealed the near absence of threading defects, corroborating the high degree of crystalline perfection in the samples, as shown in Figure 6. High resolution images of the interface indicate that the mismatch between the Ge layers and the Si wafer is accommodated by the

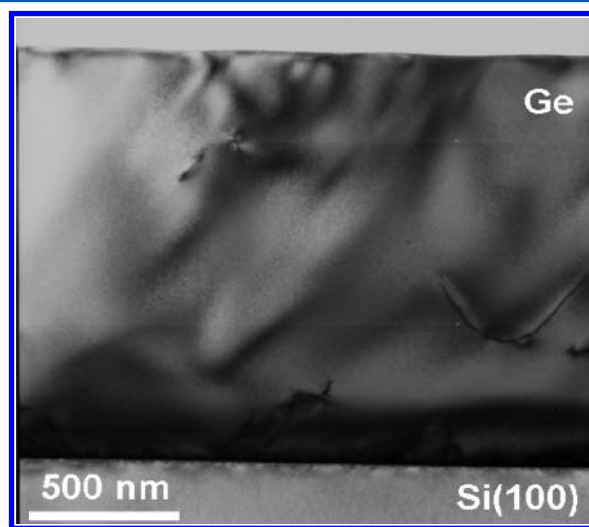


**Figure 6.** Electron micrograph showing the entire 1.5 μm Ge layer thickness of a monocrystalline film with a flat surface grown at 330 °C using trigermane.



formation of edge dislocations confined to the heterojunctions region. The outcomes indicate that our growth involving high reactivity  $\text{Ge}_3\text{H}_8$  provide a unique low temperature route enabling growth directly on Si. This, in itself, should represent a major advantage and advance in crystal growth of thick and fully relaxed films in which the majority of the volume fraction exhibits bulk-like crystal behavior.

As discussed in the introduction, in the context of Ge-based materials we have grown GeSn alloys via reactions of  $\text{Ge}_2\text{H}_6$  with  $\text{SnD}_4$  at low temperatures of 275 to 350 °C. Films with low Sn concentrations in the range of 1–3% were used to fabricate the first generation of high performance group-IV IR photodiodes with band gaps lower than that of Ge.<sup>30</sup> However, the realization of practical devices with extended capabilities into the technologically useful mid-IR range requires films possessing higher than 3% Sn contents and large thicknesses—at least 0.5–1.0  $\mu\text{m}$ —thereby ensuring an increased volume fraction of active material far from the defective interface region with Si. Unfortunately, to produce such materials using the digermane approach, the growth temperature has to be systematically reduced from 335–340 °C (at 4% Sn) to 310 °C, (at 7% Sn) to ensure full substitution of the Sn atoms in the structure. This reduction in temperature results in a concomitant decrease in growth rate, and prevents the film from relaxing the compressive strain with the mismatched Si during deposition. This, in turn, limits the overall thickness to unacceptable levels, ultimately diminishing the device potential of the materials. An immediate and practical solution to this problem is to replace  $\text{Ge}_2\text{H}_6$  with  $\text{Ge}_3\text{H}_8$ , which is more compatible with the  $\text{SnD}_4$  in terms of reactivity.

In practice, we find that this new combination of chemical sources yields a much more efficient reaction process, leading to higher growth rates at significantly lower temperatures, ultimately producing the sought-after higher-Sn-content alloys as thick crystalline layers on silicon. Our proof of principle experiments were conducted at 325–315 °C in a conventional UHV CVD reactor (described elsewhere)<sup>31</sup> using stock mixtures of ~3%  $\text{Ge}_3\text{H}_8$  and ~0.4% in high purity  $\text{H}_2$ , yielding atomically flat films as evidenced by AFM scans with rms roughness of less than 1 nm. RBS measurements showed that Sn content under the described conditions was 5–6%, and the film thickness was ~450 nm, corresponding to a growth rate of ~8–9 nm/min. As in the case of the pure Ge described, the growth rate of GeSn is improved by another factor of 3 compared to samples grown via  $\text{Ge}_2\text{H}_6$  under the same conditions, representing a significant advance in crystal growth on Si. The Rutherford backscattering spectroscopy (RBS) channelled spectra revealed that the Sn content in these samples is fully substitutional and perfectly aligned, indicating that the layer is monocrystalline and heteroepitaxial, with the underlying Si “as grown”. High resolution XRD corroborated the single crystal character and indicated the presence of a residual compressive strain, which was fully relieved by rapid thermal anneal (RTA) processing at 600 °C for 10 s. Room temperature photoluminescence (PL) experiments showed that the samples exhibit significant emission intensity in the vicinity of 1950 nm, corresponding to direct gap recombination, as shown in Figure 7, which compares the PL spectra of the  $\text{Ge}_{0.95}\text{Sn}_{0.05}$  sample with that of a 500 nm thick pure Ge film grown using tetragermane. This PL result represents the first observation of optical response from highly concentrated alloys grown on Si and can be entirely attributed to the improved crystallinity and enhanced layer thickness afforded by the new

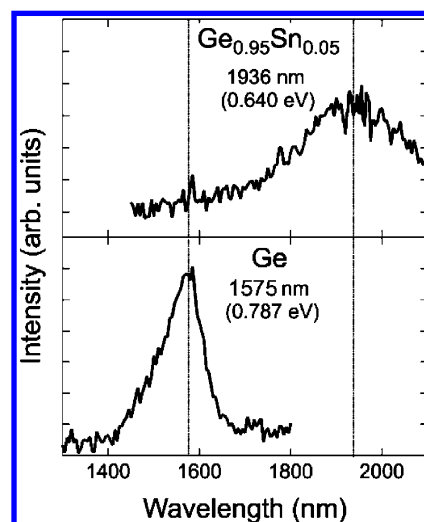


**Figure 7.** Room temperature PL spectrum of a ~500 nm thick  $\text{Ge}_{0.95}\text{Sn}_{0.05}$  layer grown directly on Si(100) using trigermane compared with the spectrum of Ge of the same thickness grown via tetragermane. The energy shift of 0.147 eV from the alloy to pure Ge corresponds to the reduction of the direct band gap due to the incorporation of Sn in the Ge lattice.

trigermane method. This favorable preliminary result has prompted us to consider extending the compositional range to 8–9% Sn and beyond using trigermane or even tetragermane. The objective is to produce structures using these materials with inherently direct gaps for applications as group IV lasers with tunable emissions integrated directly on Si.

**Growth of Ge on Si using Tetragermane.** The depositions of pure Ge films using tetragermane were performed directly on Si(100) at 310–320 °C and  $1 \times 10^{-4}$  Torr pressure, employing methods and protocols similar to those described for trigermane. The  $\text{Ge}_4\text{H}_{10}$  compound was diluted by high purity  $\text{H}_2$  to 5% by volume, allowing layer-by-layer crystal formation of thick Ge films ( $t < 0.5 \mu\text{m}$ ) at growth rates of ~20 nm/min, which are typically 2- to 3-fold greater than those observed in depositions of trigermane at the same temperature, pressure, and precursor flux. Relative to the more traditional  $\text{Ge}_2\text{H}_6$  process, this represents a marked improvement in crystal growth efficiency with all additional benefits afforded by ultra low temperature conditions. At the onset, the experiments in this case revealed that the Stranski–Krastanov mechanism that typically defines the growth of Ge on mismatched Si surfaces is completely circumvented, yielding atomically flat films over large lateral areas of at least 100  $\mu\text{m}$ . These materials were fully characterized by RBS, AFM, Nomarski optical microscopy, HR-XRD, and XTEM. The data collectively indicate that the layer morphology and crystallinity are improved relative to those of Ge films grown via trigermane and digermane. The Nomarski images showed that the layer surface was uniform, smooth, and featureless. Complementary AFM scans over  $20 \times 20 \mu\text{m}$  areas indicated an rms roughness of less than 1 nm compared to 2–3 nm values obtained in the trigermane experiments (Figure 8a). HR-XRD measurements of the (224) and (004) Bragg reflections show that the as-grown layers are monocrystalline and possess essentially strain-free structures regardless of thickness (Figure 8b). The vanishing strain may be associated with the high growth rate, as well as the enhanced reactivity and low surface mobility of the massive  $\text{Ge}_4\text{H}_{10}$  molecular cores. The samples

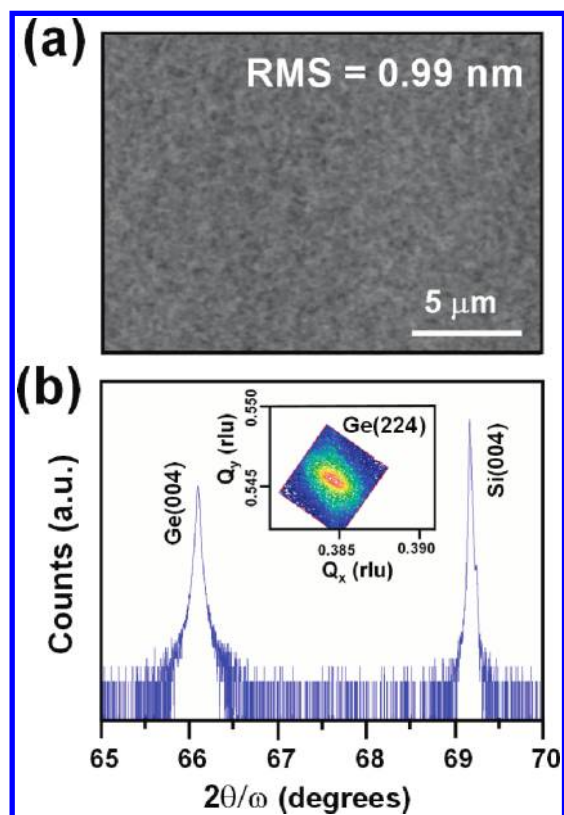


**Figure 8.** (a)  $20 \times 15 \mu\text{m}$  AFM image of a 500 nm thick Ge film showing a flat surface with smooth morphology. (b) High resolution X-ray plots showing the on-axis (004) peaks and the off-axis (224) reciprocal space map (inset). The data confirms that the film are monocrystalline and essentially strain-free as grown (fwhm of the (004) rocking curve is 215 arcseconds).

exhibit relatively narrow (004) rocking curves with a typical fwhm of 600 arcseconds, indicating a relatively narrow mosaic spread. This is significantly improved by RTA processing at  $725^\circ\text{C}$  for 10 s. The procedure markedly sharpens the XRD peak, leading to a reduction of the fwhm down to 250 arcseconds. This value is on par with the best observed to date for state-of-the-art Ge-on-Si samples, which typically possess thicknesses larger than those of the current samples. RBS ion channeling revealed a high degree of epitaxial alignment in the as-grown samples, which was also significantly improved upon RTA processing. XTEM micrographs obtained from the annealed samples show uniform films exhibiting flat surfaces. The bulk layers are found to be largely devoid of threading defects as illustrated by the micrograph of Figure 9. High resolution images revealed periodic arrays of misfit dislocations that are confined to the interface plane and absorb the strain differential between the epilayer and the substrate (Figure 9). The results here suggest that the tetragermane-based approach described can be used to deposit device quality GeSn alloys with high Sn contents, improved crystallographic and morphological properties, and, most importantly, bulk-like thicknesses in the several micrometer range.

### 3. CONCLUSIONS

In analogy to the related Si and Si–Ge counterparts, in this work, we introduce viable preparations of trigermane ( $\text{Ge}_3\text{H}_8$ ) and tetragermane ( $\text{Ge}_4\text{H}_{10}$ ) for applications in semiconductor materials science and technology. The compounds are

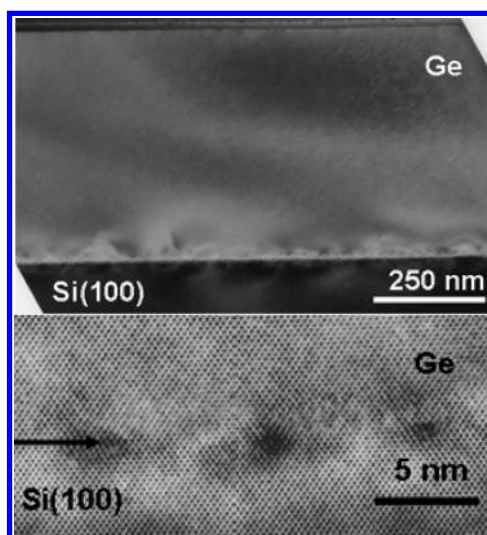


**Figure 9.** XTEM images of Ge/Si(100) sample grown at  $320^\circ\text{C}$  using tetragermane. (top) The entire 500 nm film thickness is shown within the field of view indicating that the epilayer is largely devoid of threading defects. (bottom) Corresponding high resolution image showing edge type dislocations confined within the interface plane marked by the arrow.

produced in relatively high yield and purity via thermolysis of  $\text{Ge}_2\text{H}_6$ , as implemented in a flow through reaction arrangement. They are thoroughly characterized using spectroscopic methods and first-principles quantum simulations, which provide detailed new information concerning the molecular properties and stability range, which had remained elusive to date. A key conceptual motivation of the work is the potential of these heavy hydride chemical sources to dramatically expand the functionality of group IV devices comprising of Ge-based architectures. This is achieved by lowering the process temperatures while increasing the crystal growth rate in selective and blanket growth, thereby allowing the formation of metastable structures and alloy compositions not accessible using conventional methods.

Here, we demonstrate the viability of this ultra-low-temperature strategy by producing optical quality Ge and  $\text{Ge}_{1-x}\text{Sn}_x$  directly on Si, using both  $\text{Ge}_3\text{H}_8$  and  $\text{Ge}_4\text{H}_{10}$ . The new approach yields monocrystalline films at unprecedented temperatures in the range  $300\text{--}330^\circ\text{C}$ , at scalable growth rates amenable to industrial throughput levels. The preliminary results show that the traditional island-like growth mode (Stranski–Krastanov) is completely suppressed, allowing the formation of uniform layers with flat surfaces and completely relaxed microstructures. Samples of thickness of  $1.5 \mu\text{m}$  and beyond can be routinely produced using trigermane, providing access to bulk-like materials, as needed for applications in photonics, including photovoltaics. In this regard, the experiments using the more reactive tetragermane show that this compound provides the most straightforward and efficient pathway to the growth on Ge on Si, suggesting that any further gains will be difficult to realize using chemical means. (**Cautionary note:** In our hands, the compounds reported in this paper were handled under inert conditions in glass vessels with no discernible instabilities. Nevertheless, under certain conditions, digermane (a commercial chemical) has been alleged to unexpectedly and violently decompose via instantaneous release of  $\text{H}_2$ . Accordingly, special care should be taken in dealing with these related compounds.)

## ■ ASSOCIATED CONTENT

### ● Supporting Information

Diagram of the reactor used to produce trigermene through pyrolysis of digermene according to the reaction:  $2\text{Ge}_2\text{H}_6 \rightarrow \text{GeH}_4 + \text{Ge}_3\text{H}_8$  at 250 °C. This information is available free of charge via the Internet at <http://pubs.acs.org/>.

## ■ AUTHOR INFORMATION

### Notes

The authors declare no competing financial interest.

## ■ ACKNOWLEDGMENTS

This work was supported by the U.S. Air Force under contract no. DOD AFOSR FA9550-06-01-0442 (MURI program), by the Department of Energy under contract no. DE-FG36-08GO18003, and by the National Science Foundation under grant no. DMR-0907600.

## ■ REFERENCES

- (1) Thomas, S. G.; Bauer, M.; Stephens, M.; Kouvetakis, J. *Solid State Technol.* **2009**, 52, 12.
- (2) Green, M. A. *Prog. Photovoltaics* **2001**, 9, 123.
- (3) Beeler, R. T.; Grzybowski, G. J.; Roucka, R.; Jiang, L.; Mathews, J.; Smith, D. J.; Menéndez, J.; Chizmeshya, A. V. G.; Kouvetakis, J. *Chem. Mater.* **2011**, 23, 4480.
- (4) Xie, J.; Chizmeshya, A. V. G.; Tolle, J.; D'Costa, V. R.; Menéndez, J.; Kouvetakis, J. *Chem. Mater.* **2010**, 22, 3779.
- (5) Vincent, B.; Gencarelli, F.; Bender, H.; Merckling, C.; Douhard, B.; Petersen, D. H.; Hansen, O.; Henrichsen, H. H.; Meersschart, J.; Vandervorst, W.; Heyns, M.; Loo, R.; Caymax, M. *Appl. Phys. Lett.* **2011**, 99, 152103.
- (6) Kouvetakis, J.; Mathews, J.; Roucka, R.; Chizmeshya, A. V. G.; Tolle, J.; Menéndez, J. *IEEE Photonics J.* **2010**, 2, 924.
- (7) Fang, Y.-Y.; Tolle, J.; D'Costa, V. R.; Menendez, J.; Chizmeshya, A. V. G.; Kouvetakis, J. *Chem. Mater.* **2007**, 19, 5910.
- (8) Luan, H.-C.; Lim, D. R.; Lee, K. K.; Chen, K. M.; Sandland, J. G.; Wada, K.; Kimerling, L. C. *Appl. Phys. Lett.* **1999**, 75, 2909.
- (9) Michel, J.; Liu, J.; Kimerling, L. C. *Nat. Photonics* **2010**, 4, 527.
- (10) Shang, H.; Frank, M. M.; Gusev, E. P.; Chu, J. O.; Bedell, S. W.; Guarini, K. W.; Jeong, M. *IBM J. Res. Dev.* **2006**, 50/4–5, 377.
- (11) Liu, J. F.; Michel, J.; Giziewicz, W.; Pan, D.; Wada, K.; Cannon, D. D.; Jongthammanurak, S.; Danielson, D. T.; Kimerling, L. C.; Chen, J.; Ilday, F. O.; Kartner, F. X.; Yasaitis, J. *Appl. Phys. Lett.* **2005**, 87, 103501.
- (12) Kuo, Y. H.; Lee, Y. K.; Ge, Y. S.; Ren, S.; Roth, J. E.; Kamins, T. I.; Miller, D. A. B.; Harris, J. S. *Nature* **2005**, 437, 1334.
- (13) Liu, J.; Sun, X.; Camacho-Aguilera, R.; Kimerling, L. C.; Michel, J. *Opt. Lett.* **2010**, 35, 679.
- (14) Chung, K. H.; Yao, N.; Benziger, J.; Sturm, J. C.; Singh, K. K.; Carlson, D.; Kuppuraio, S. *Appl. Phys. Lett.* **2008**, 92, 113506.
- (15) Fitzgerald, E. A.; Samavedam, S. B. *Thin Solid Films* **1997**, 294, 3.
- (16) Fischer, P. R.; Aerde, S. V.; Oosterlaken, E.; Bozon, B.; Zagwijn, P. M.; Bauer, M.; Yan, M.; Verweij, W. *ECS Trans.* **2006**, 3/2, 203.
- (17) Fang, Y.-Y.; D'Costa, V. R.; Tolle, J.; Poweleit, C. D.; Kouvetakis, J.; Menéndez, J. *Thin Solid Films* **2008**, 516, 8327.
- (18) Drake, J. E.; Jolly, W. L. *Inorg. Synth.* **1963**, 7, 34.
- (19) Drake, J. E.; Jolly, W. L. *J. Chem. Soc.* **1962**, 2807.
- (20) Mackay, K. M.; Sutton, K. J. *J. Chem. Soc.* **1968**, 2312.
- (21) Mackay, K. M.; Robinson, P. *J. Chem. Soc.* **1965**, 5121.
- (22) Estacio, P.; Sefcik, M. D.; Chan, E. K.; Ring, M. A. *Inorg. Chem.* **1970**, 9, 1068.
- (23) Boourasseau C. U.S. Patent Application US 2008/0175784 A1; Pub. Date: Jul. 24, 2008.
- (24) Ritter, C. J.; Hu, C.-W.; Chizmeshya, A. V. G.; Tolle, J.; Klewer, D.; Tsong, I. S. T.; Kouvetakis, J. *J. Am. Chem. Soc.* **2005**, 127, 9855.
- (25) Ritter, C. J.; Hu, C.-W.; Chizmeshya, A. V. G.; Tolle, J.; Nieman, R.; Tsong, I. S. T.; Kouvetakis, J. *J. Am. Chem. Soc.* **2006**, 128, 6919.
- (26) Frisch, M. J.; Trucks, G. W.; Schlegel, H. B.; Scuseria, G. E.; Robb, M. A.; Cheeseman, J. R.; Montgomery, J. A., Jr.; Vreven, T.; Kudin, K. N.; Burant, J. C.; Millam, J. M.; Iyengar, S. S.; Tomasi, J.; Barone, V.; Mennucci, B.; Cossi, M.; Scalmani, G.; Rega, N.; Petersson, G. A.; Nakatsuji, H.; Hada, M.; Ehara, M.; Toyota, K.; Fukuda, R.; Hasegawa, J.; Ishida, M.; Nakajima, T.; Honda, Y.; Kitao, O.; Nakai, H.; Klene, M.; Li, X.; Knox, J. E.; Hratchian, H. P.; Cross, J. B.; Bakken, V.; Adamo, C.; Jaramillo, J.; Gomperts, R.; Stratmann, R. E.; Yazyev, O.; Austin, A. J.; Cammi, R.; Pomelli, C.; Ochterski, J. W.; Ayala, P. Y.; Morokuma, K.; Voth, G. A.; Salvador, P.; Dannenberg, J. J.; Zakrzewski, V. G.; Dapprich, S.; Daniels, A. D.; Strain, M. C.; Farkas, O.; Malick, D. K.; Rabuck, A. D.; Raghavachari, K.; Foresman, J. B.; Ortiz, J. V.; Cui, Q.; Baboul, A. G.; Clifford, S.; J. Cioslowski, B. B. Stefanov, G. Liu, A. Liashenko, P. Piskorz, I. Komaromi, R. L. Martin, D. J. Fox, T. Keith, M. A. Al-Laham, C. Y. Peng, A. Nanayakkara, M. Challacombe, P. M. W. Gill, B. Johnson, W. Chen, M. W. Wong, C. Gonzalez, Pople, J. A. *Gaussian 03*, Revision C.02; Gaussian, Inc.: Wallingford, CT, 2004.
- (27) Weng, C.; Kouvetakis, J.; Chizmeshya, A. V. G. *J. Comput. Chem.* **2011**, 32 (5), 835.
- (28) Chen, S. S.; Wilhoit, R. C.; Zolinski, B. J. *J. Phys. Chem. Ref. Data* **1975**, 4 (4), 859.
- (29) Wistey, M.; Fang, Y.-Y.; Tolle, J.; Chizmeshya, A. V. G.; Kouvetakis, J. *Appl. Phys. Lett.* **2007**, 90, 082108.
- (30) Roucka, R.; Mathews, J.; Weng, C.; Beeler, R.; Tolle, J.; Menéndez, J.; Kouvetakis, J. *IEEE J. Quantum Electron.* **2011**, 47, 213.
- (31) D'Costa, V. R.; Fang, Y.-Y.; Mathews, J.; Roucka, R.; Tolle, J.; Kouvetakis, J.; Menéndez, J. *Semicond. Sci. Technol.* **2009**, 24, 115006.